Meteorologische Zeitschrift, Fast Track DOI: 10.1127/0941-2948/2013/0441


**Open Access Article**

# Size-resolved flux measurement of sub-micrometer particles over an urban area

MALTE JULIAN DEVENTER[1]*, FRANK GRIESSBAUM[1,2] and OTTO KLEMM[1]

[1]Institute of Landscape Ecology - Climatology Working Group, Westfälische Wilhelms-Universität Münster, Münster, Germany
[2]now at LI-COR Biosciences GmbH, Bad Homburg, Germany

(Manuscript received December 31, 2012; in revised form June 6, 2013; accepted June 6, 2013)

**Abstract**

From April 11th to May 27th, 2011, the turbulent exchange of sub-micrometer particles between the urban surface and the urban boundary-layer was measured above the city area of Münster (NW Germany). The scope of the study is to examine the contributions of particles of different size classes to the total measured fluxes. Eddy-covariance measurements were performed at 65 m above ground. The particle concentrations in 99 size bins with particle diameters ranging from 55 to 1000 nm were measured with an optical particle spectrometer. For flux calculations we grouped these 99 original bins into 18 wider channels with an upper cut-off of 320 nm, and a further rather coarse channel for particles up to 1 μm. The overall results reveal that Münster is a relevant source of about $2.8 \cdot 10^8$ particles $m^{-2}$ $d^{-1}$ on weekdays and $1.8 \cdot 10^8$ particles $m^{-2}$ $d^{-1}$ on Sundays within the indicated size range. These emissions are predominantly driven by secondary particles of the Aitken mode, which are most likely caused by traffic. Hence traffic hotspots are a major contribution to the net fluxes. On the other hand, considering the mass fluxes, Münster is a sink of 0.53 μg $m^{-2}$ $d^{-1}$ on weekdays and 0.08 μg $m^{-2}$ $d^{-1}$ on Sundays. Here, mainly particles of the accumulation mode with diameters above 167 nm lead to deposition fluxes. Number and mass fluxes exhibit distinct daily and weekly patterns.

**Keywords:** urban aerosol, size-resolved aerosol flux.

## 1 Introduction

A profound understanding of the role of aerosol particles in atmospheric processes becomes increasingly important in terms of ongoing global warming and global and meso-scale modeling. For instance, the current knowledge of a net cooling effect, resulting from direct back scattering of solar radiation and from indirect effects through particles acting as cloud condensation nuclei (CCN), suffers from considerable uncertainties (IPCC, 2007). Moreover, toxicological and epidemiological studies have identified correlations between ambient particulate matter concentrations and adverse health effects (MAUDERLY and CHOW, 2008) emphasizing the importance of further investigation and monitoring of aerosol particle dynamics especially in densely populated regions.

Among others, the identification and quantification of source and sink mechanisms of particulate material (PM) needs detailed analysis. The PM concentrations in many cities of the European Union exceed the current legal limits. In principle, there are two concepts that can be used to study the sources of urban PM. Firstly, source apportionment studies of urban PM based on chemical analysis revealed that the particle mass originates both from inner-urban sources and from advection from more distant sources (SWIETLICKI et al., 1996; QUEROL et al., 2001; GIETL and KLEMM, 2009). Secondly, direct flux measurements revealed that cities act mainly as sources for aerosol particles. Most flux studies showed significant correlations between particle number fluxes ($F_n$) and traffic activity with synchronous diurnal patterns peaking at rush hours (NEMITZ et al., 2000; MÅRTENSSON et al., 2006; JÄRVI et al., 2009; MARTIN et al., 2009; DAHLKÖTTER et al., 2010; VOGT et al., 2011a; HARRISON et al. 2011). They also identified higher flux densities for footprints representing industrial or traffic-affected areas as compared to rural areas. So far, all surveyed cities have been identified as ultrafine particle (UFP) sources with positive daily $F_n$ cycles, while deposition fluxes are reported to only occur at times with low particle loadings (MÅRTENSSON et al., 2006; HARRISON et al., 2011). However, these two concepts have not yet yielded consistent results.

The answer could lie in a size-resolved examination of aerosol particle fluxes. An emission of ultrafine particles from an urban environment might occur simultaneously with a net input of particle mass, embodied by larger particles.

*Corresponding author: Malte Julian Deventer, Institute of Landscape Ecology - Climatology Working Group, Westfälische Wilhelms-Universität Münster, Schlossplatz 2, 48149 Münster, Germany, e-mail: julian.deventer@uni-muenster.de

DOI 10.1127/0941-2948/2013/0441
0941-2948/2013/0441 $ 4.05

The first results from studies with size resolved aerosol particle measurements indicate differences between the fluxes of different particle size classes (SCHMIDT and KLEMM, 2008). Using the disjunct eddy covariance method and a 12-stage electrical low pressure impactor (ELPI), those authors claim a positive mean $F_n$ and a simultaneously occurring negative mass flux ($F_m$). The present study presents a much further developed approach through the use of a faster particle spectrometer in combination with directly applied and highly size resolved eddy covariance (EC) measurements. Can urban agglomerations act as sinks for larger particles and eventually of particle mass? Is this assumption feasible considering the background of high net emission of high particle numbers from cities?

# 2 Method

## 2.1 Measurement site

The study was carried out between 11th of April and 27th of May 2011 in the city of Münster (NW Germany). The spring of 2011 proved to be above-average warm and dry (+5/+2 °C, −52/−66 mm for the months of April and May compared with the multi-annual means), with monthly mean temperatures of 14 °C and 15 °C, and monthly precipitation totals of 28 mm and 33 mm, respectively.

Measurements were taken on a 62 m high radio tower located in a military base, southeast of the city center. The combination of prevailing westerly winds and the tower location provides a frequent representation of urban footprints in the measurements. The site surroundings are roughly divisible into three different land use classes (see Fig. 1). Sector 1 (90° (E) to 180° (S)) is a rural and heterogeneous sector, mostly covered by agricultural land and suburbs. However, a busy bypass road and an inland waterway run through this sector. The densely developed urban sector 2 (180° to 225°) contains major traffic infrastructure such as parts of the main railway station and an inland harbor, as well as industrial areas and a major power plant. The most important emission sources of this sector are traffic and large industrial smokestacks. Sector 3 (225° to 0°) comprises mainly residential areas and the city center as well as traffic hotspots. Data from wind directions between 0° (N) and 90° (E) were discarded due to a possible disturbance of the sonic anemometer by other instruments. The nearest (< 1 km) periphery of the tower is dominated by three-storied residential buildings of 15–20 m height, and 2 busy roads. All instruments were mounted at least 40 m above the surrounding rooftops, so that the direct influence of point sources such as air vents was unlikely. Furthermore, emissions from wood burning can be expected to be marginal due to the mild spring. The site characterization and results from preliminary studies (GIETL et al., 2008; DAHLKÖTTER et al., 2010) lead us to the conclusion that the measurement site is mostly influenced by traffic, industry, and the long range transport of aerosol particles. For a more detailed site description, see GRIESSBAUM and SCHMIDT (2009).

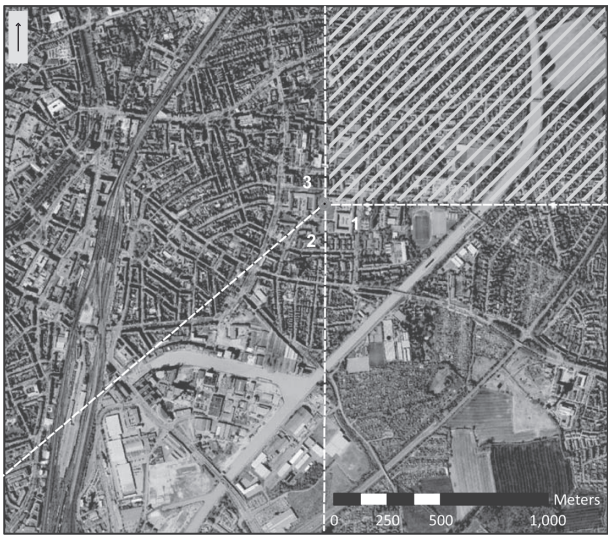


**Figure 1:** Satellite image of the study area. Overlaid on the map are the three different land use sectors: (1) rural-suburban, (2) industry-traffic and (3) residential-traffic. Data from the shaded sector was not used due to distortion of the sonic anemometer measurement. Graphics source: © 2013 AeroWest Digital Globe, GeoBasis-DE/BKG, GeoContent. Mapdata: © 2013 GeoBasis-DE/BKG, 2009 © Google Maps.

Footprints, as calculated with the FSAMW model (SCHMID, 1994), showed a high spatial representativeness of the urban footprint areas with sizes ranging from 0.1 $km^2$ during unstable, and up to 6.5 $km^2$ during stable boundary layer regimes. The model footprints only showed source sector 1 (between 90° and 180°) to be outside of the urban area. Thus we used this more rurally stamped sector for an urban-rural comparison. However, the calculated footprints and the spatial flux analysis are only of indicative character, since the performance of footprint models has not yet been rigorously tested for complex and heterogeneous surfaces such as cities. To relate the particle concentrations to traffic volume, we divided the data into two groups; the first group containing samples from weekdays (including Saturdays), the second representing Sundays. One public holiday on a Tuesday was discarded while the second holiday coincided with a Sunday.

## 2.2 Instrumentation

The EC setup consisted of an R3-50 Ultrasonic Anemometer (Gill Instruments Ltd., Lymington, Hampshire SO41 9EG, UK), a LI-7500 Open Path $CO_2/H_2O$ Infrared Gas Analyzer (LI-COR Inc., Lincoln, Nebraska 68504, USA), and an Ultra-High Sensitivity Aerosol Spectrometer (UHSAS, Droplet Measurement Technologies, Boulder, CO, USA) which measures particle concentrations in the 0.055–1 μm diameter size range.

**Table 1:** Channel Overview: $D_m$ = geometric mean diameter, $D_u$ = upper channel boundary, and Eff. = collection efficiency.

| | $D_m$ [nm] | $D_u$ [nm] | Eff. [%] |
|---|---|---|---|
| 1 | 57,5 | 60,1 | 83,2 |
| 2 | 62,7 | 65,6 | 84,8 |
| 3 | 68,5 | 71,6 | 86,2 |
| 4 | 74,8 | 78,2 | 87,5 |
| 5 | 81,7 | 85,4 | 88,7 |
| 6 | 89,2 | 93,2 | 89,7 |
| 7 | 97,4 | 101,8 | 90,6 |
| 8 | 106,3 | 111,1 | 91,5 |
| 9 | 116,1 | 121,3 | 92,3 |
| 10 | 126,8 | 132,5 | 92,9 |
| 11 | 138,4 | 144,6 | 93,6 |
| 12 | 151,1 | 157,9 | 94,1 |
| 13 | 167,4 | 177,5 | 94,7 |
| 14 | 188,3 | 199,6 | 95,3 |
| 15 | 211,7 | 224,4 | 95,8 |
| 16 | 238 | 252,3 | 96,2 |
| 17 | 267,6 | 283,7 | 96,6 |
| 18 | 300,8 | 319 | 97 |
| 19 | 564,8 | 1000 | 98,2 |

The spectrometer illuminates the sampled particles with a solid state laser and performs single particle sizing of up to 99 size bins as a function of the intensity of scattered light. All measurement sensors and the tube inlets were installed 3 m above the topmost platform of the radio tower, resulting in a total measurement height of 65 m above ground level. Prior to the measurement campaign, the UHSAS was calibrated with DUKE Polymer Microsphere standards. All sensors were recorded with a minimum of 10 Hz frequency.

For particle measurements, the sampled air was aspirated through TYGON tubing of 2.7 m length and 1/16 inch (about 1.6 mm) inner diameter with a sample flow rate of 0.83 $cm^3\ s^{-1}$. This resulted in Reynolds numbers of $0.002 < Re < 0.02$. Particle losses in the tubing were estimated in accordance with BARON and WILLEKE (2005). The OPC was placed perpendicularly to the sonic anemometer to ensure vertical alignment with the exception of the curved inlet. Gravitational settling as well as losses in bent sections play only minor roles for the sub-micrometer particles. Most of the particle losses are caused by diffusion (Table 1).

## 2.3 Uncertainties

The maximum achievable particle size resolution for EC was limited by statistical uncertainties in combination with instrument limitations (TAYLOR, 1982; FAIRALL, 1984; LENSCHOW and KRISTENSEN, 1984; BUZORIUS et al., 2003). A minimum of 10 particles per 0.1 s should be analyzed in each size bin. The instrument manufacturer set a maximum detection limit of 300 particles per 0.1 s for the entire measurement range, which simultaneously limits the sample flow rate. On the other hand, the particle concentrations are highly variable with time. It had to be ensured that during low-concentration periods a sufficient amount of particles was sampled within every channel. To meet all restrictions to an optimal degree, we combined the initial number of 99 size bins into 18 wider channels with an upper cut-off of 320 nm, and a further rather coarse channel for particles up to 1 μm (Table 1).

Uncertainties in number concentration measurements due to discrete counting (HINDS, 1999) and the relative flux uncertainty due to limited counting statistics (BUZORIUS et al., 2003) were calculated according to

$$\delta(\mathrm{N}) = \frac{1}{\sqrt{\mathrm{N}}}, \tag{1}$$

where δ(N) is the uncertainty in number concentration [%] and N is the sum of counts for a whole averaging interval, and

$$\delta\left(\overline{\mathrm{w'c'}}\right) = \frac{\sigma_\mathrm{w}\bar{c}}{\sqrt{\mathrm{N}}\left(\overline{\mathrm{w'c'}}\right)}, \tag{2}$$

where $\delta(\overline{w'c'})$ is the relative uncertainty of the number flux [%], $\sigma_w$ the standard deviation of the vertical wind component [m $s^{-1}$], $\bar{c}$ the mean number concentration [particles $m^{-3}$], and $(\overline{w'c'})$ the number flux [particles $m^{-2}\ s^{-1}$].

Concentration uncertainties δ(N) range from 0.22% for the smaller channels up to 0.39% for the bigger channels. Slightly lower values were recently reported by AHLM et al. (2010) and VOGT et al. (2011b), both using the GRIMM OPC 1.109. Flux uncertainties, $\delta(\overline{w'c'})$ are comparably low for channels with $D_m < 100$ nm, but significantly increase for channels with $D_m$ up to 167 nm (Ch. 13). For channels with $D_m > 167$ nm, the median $\delta(\overline{w'c'})$ fluctuates around 50% (see Fig. 2). High uncertainties are a result of periods in which $F_n$ are low, or in which a high particle ambient concentration is decoupled from $F_n$, meaning that $\frac{\bar{c}}{(\overline{w'c'})}$ increases.

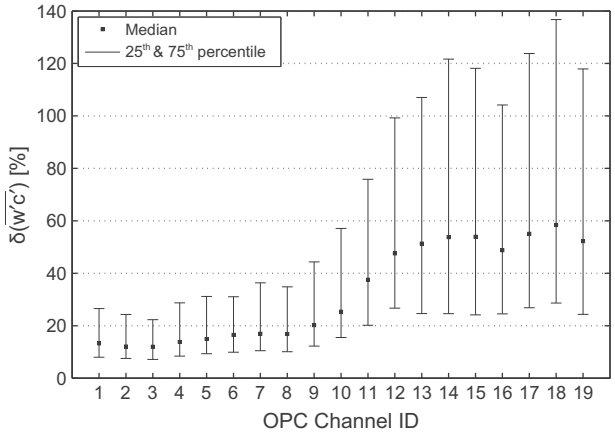


**Figure 2:** Median and 25th/75th percentiles of relative flux uncertainty $\delta(\overline{w'c'})$.

## 2.4 Mass fluxes

For the conversion from number fluxes ($F_n$) to mass fluxes ($F_m$), we assume spherical particle shape and a uniform density of $1.6 \cdot 10^{12}$ µg m$^{-3}$. For each channel, we calculate a single spherical particle volume [m$^{-3}$] based on mean diameter. Furthermore, we multiply this mean volume with the fixed density, resulting in a mean particle mass [µg] for one particle of each channel. Finally, we multiply this mass with the number fluxes [particles m$^{-2}$ s$^{-1}$] to estimate the mass fluxes for a specific averaging interval [µg m$^{-2}$ s$^{-1}$]. It is known that PM density shows both daily and seasonal variations which are driven, among other factors, by chemical composition, particularly by the fraction of black carbon. As it is not feasible to specify the exact mass of the sampled PM with the instruments employed in this study, we use the mean value for the density of $PM_{2.5}$ from PITZ et al. (2003) with a standard deviation of $\pm 0.5 \cdot 10^{12}$ g m$^{-3}$, which is based on daily urban samples from nearly 2 years of data. Consequently this standard deviation reflects the hourly, day to day as well as seasonal variability of the particle density.

During the computation of the mass flux for particles with diameter > 319 nm (channel 19), the variability of the size distribution within this channel needs to be taken into account. Artifacts from poor counting statistics at the upper end of the channels must be minimized. We first calculate masses for the original 40 channels within this range. The sum of the 40 channels' masses is then divided by the total count of the 40 channels, which results in the average mass of 1 particle in channel 19. Finally, we multiply the total number flux in channel 19 with the associated mass estimate. This procedure is performed for each 30 minute interval. The average particle mass (0.84 µg) is highly variable (interquartile range 0.63 µg – 0.96 µg), reflecting considerable changes in the size distribution.

In conclusion, the described conversion from $F_n$ to $F_m$ is an approximation of the real mass flux. Hence, our mass fluxes entail higher uncertainties than the directly measured Fn.

## 2.5 Post processing

The analysis of ogive functions (FOKEN and WICHURA, 1996, not presented in detail) shows that all frequency scales with a relevant contribution to the turbulent transport of particles are captured at an averaging interval of 30 minutes, which was used for all flux calculations in this study.

We applied the following correction procedures for the eddy covariance computation: correction for particle losses in the tubing (Table 1), plausibility checks with defined limit values, lag correction by computing the cross-correlation function, de-spiking with interpolated replacement (VICKERS and MAHRT, 1997), 2-D tilt correction of the sonic anemometer, Webb-Pearman-Leuning correction (WEBB et al., 1980), and linear de-trending. Subsequently, a quality control scheme was used to filter out data which failed a test on stationarity (FOKEN and WICHURA, 1996), on the integral turbulence characteristic (FOKEN and WICHURA, 1996), on wind direction (see section 2.1), and stability (here: friction velocity > 0.1 m s$^{-1}$ and the Monin-Obukhov stability parameter < 0.16), respectively. The remaining set of high quality data covers 55% of the experimental period.

**Table 2:** Arithmetic mean $\bar{c}$ and median $\tilde{c}$ concentrations for particles in the 100–500 nm size range for three measurement sites situated in Germany (GER) and the Netherlands (NL).

| Station | Country | Instrument | [cm$^{-3}$] | [cm$^{-3}$] |
|---|---|---|---|---|
| Cabauw | NL | SMPS | 1240 | 952 |
| Boesel | GER | SMPS | 1428 | 1250 |
| Münster | GER | UHSAS | 1187 | 1157 |

# 3 Results and discussion

To put our data into context, we compared the measured number concentrations to EUCAARI, EUSAR and GUAN inventories as presented by ASMI et al. (2011). For a better comparability, we focused on the two nearest sites Cabauw (Netherlands) and Bösel (Germany) and the parameter N100, representing particle concentrations in the 100–500 nm size range. The SMPS data of the 2 reference sites are in good agreement to our OPC data (see Table 2).

Overall, the city of Münster acted as a relevant source of particles with an average daily emission of $2.49 \cdot 10^8$ m$^{-2}$ during the week, and $1.82 \cdot 10^8$ m$^{-2}$ on Sundays, respectively. However, considering the aerosol mass flux $F_m$, Münster was a sink of 1.39 µg m$^{-2}$ (weekdays) and 0.34 µg m$^{-2}$ on Sundays. The highly size-resolved approach applied here explains the cause for these seemingly contradictory results.

## 3.1 Number fluxes

The average daily pattern (Fig. 3a) of the total number flux exhibits a steep increase in fluxes beginning in the early morning at around 06:00. This is in good agreement with other studies which found strict correlations between the daily course of UFP and traffic intensity (DORSEY et al, 2002; MÅRTENSSON et al., 2006; JÄRVI et al., 2009; MARTIN et al., 2009; DAHLKÖTTER et al., 2010; VOGT et al., 2011a). Our data show a maximum of upward fluxes around 11:00. From then on, the fluxes remain at a high level throughout noontime and show a continuous decrease during the evening hours with near-zero values through the night. The time delay between the local rush-hour time of 07:00 and peak

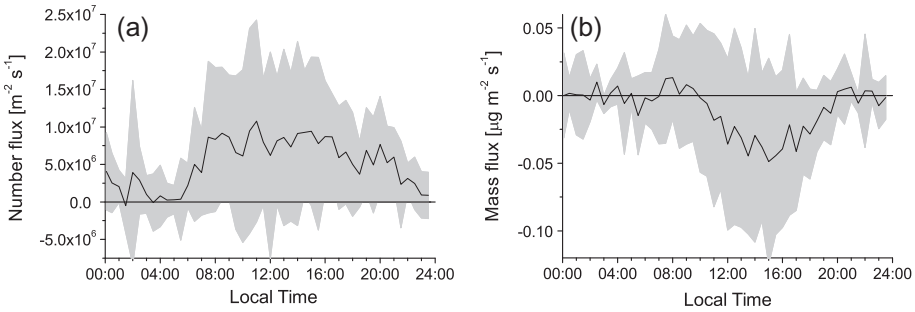


**Figure 3:** Average diurnal cycle of (a) number fluxes and (b) mass fluxes over all channels. The grey area symbolizes ±1 standard deviation.

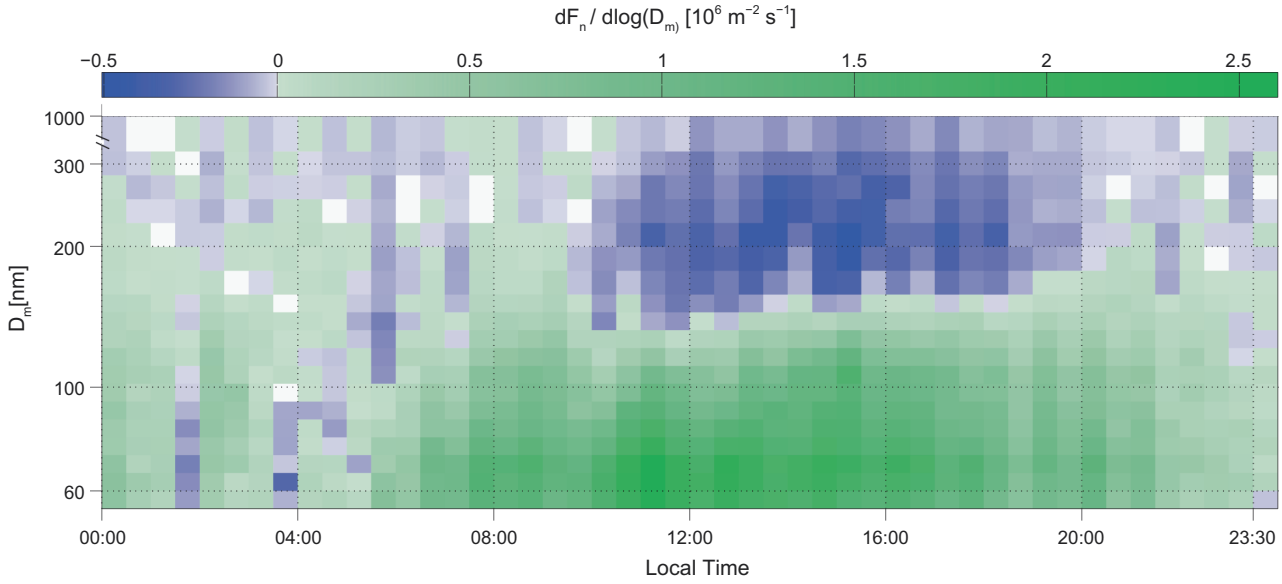


**Figure 4:** Mean daily number fluxes, normalized with the logarithm of the channel width, for all UHSAS channels. Y-axes is a log scale and non-continuous.

fluxes at 11:00 is probably due to the generally lower turbulence and shallower boundary layers in the morning and the concentration patterns of the particles observed at the study area. Hence, emitted particles accumulate within the boundary layer and near-surface concentrations peak at 08:00. Afterwards, the turbulence (here approximated by momentum flux) increases towards a midday peak. From theory and earlier observations (not shown), it is evident that the boundary layer height exhibits a similar behavior when solar heating of the surface is present. During the afternoon, efficient turbulent transport occurs, the mixed layer grows and particle concentrations decline while the fluxes increase.

The above described daily patterns and the considerably lower fluxes on Sundays as compared to workday emissions confirm the dominating role of traffic to the observed particle number emission.

Most previous urban flux studies refer to total number fluxes of all sizes covered by the employed particle counter. Our size-resolved flux measurement identified a reversal of the flux direction with increasing particle diameter, resulting in the occurrence of bi-directional fluxes. Particle number fluxes ($F_n$) are driven by the Aitken mode particles (green color in Fig. 4). The tipping point – defined as the particle size class with fluxes closest to zero – lies at 167 nm (channel 13). Fluxes of bigger particles are mostly negative (blue color in Fig. 4). The major contribution to emission originates from particles of $D_m$ = 63 nm (channel 2), and at the same time, the greatest contribution to deposition originates from particles of $D_m$ = 268 nm (channel 17).

The largest deposition fluxes occur mostly in the afternoon at around 14:00–16:00 with a time delay of 4 hours after the peak of number emissions. It may be hypothesized that the negative fluxes in the afternoon result from downward mixing of the previously emitted UFP. However, recently reported growth rates of 1–20 nm h$^{-1}$ for urban aerosols (KULMALA et al., 2004; SALMA et al., 2011) in combination with the time delay between emission and deposition peaks are too small to cause the observed deposition. Therefore, the downward mixed particles must be longer lived ones that were formed

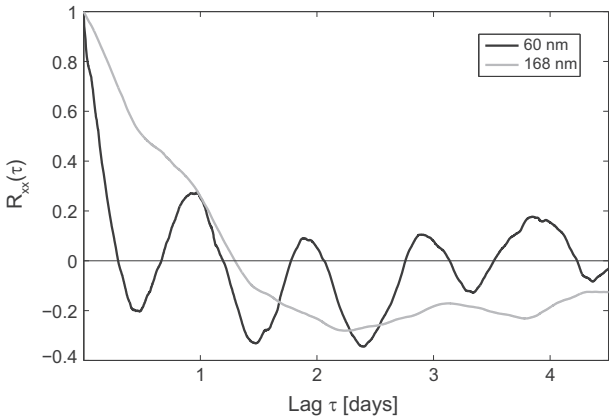


**Figure 5:** Autocorrelation function of particle concentrations for 2 different size classes.

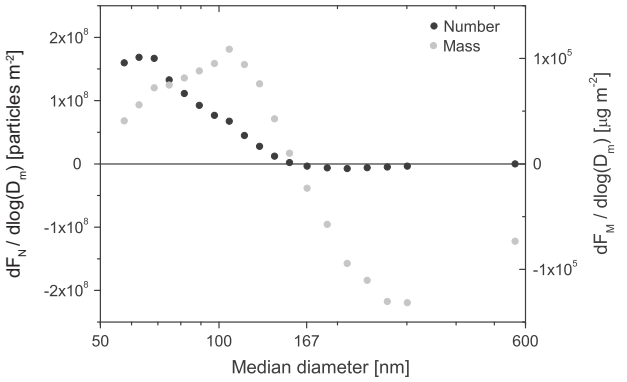


**Figure 6:** Normalized flux distribution during the entire measurement campaign for all 19 UHSAS channels. X-axis in log scale; mass fluxes (grey dots), number fluxes (black dots).

during the previous days. They probably remained in the residual layer or were previously transported over a long distance to the study area. With typical nightly wind speeds of 3–5 m $s^{-1}$, emitted particles from the nearby Ruhr area (Germany's highest populated area, 70+ km distance upwind) could easily reach the study site within one day. This suggests that meso-scale advection and down-mixing of particles which were formed one or more days earlier, are the main drivers for particle deposition.

To further investigate the dynamics of differently sized particles, we analyzed various autocorrelation functions (ACF) of particle concentrations as well as the integral time scale (τe), which is the integration of the ACF (starting at 1 for lag τ = 0) up to the first crossing of $\frac{1}{e}$ = 0.369. The ACF for particles < 167 nm shows a distinct periodicity with peaks at time shifts of multiples of 1 day (Fig. 5). For these channels, the integral time scales (τe) are within 2–3 hours. With increasing particle diameter the periodic behavior becomes less pronounced and τe values become significantly larger (up to ½ day). The concentrations of larger particles are of a more persistent nature. This confirms the analysis mentioned above that temporal scales longer than one day drive the dynamics of the larger particles. While the diurnal patterns of the small particles can best be explained by urban processes, mainly traffic, the bigger particles are most likely associated with meso-scale air mass transport.

## 3.2 Mass fluxes

While the number fluxes, $F_n$ are driven by UFP, the negative mass fluxes, $F_m$ are primarily established through particles larger than the Aitken mode. Given the cubic growth of volume and thus mass by diameter, and given the more frequently observed downward transport of the larger particles, their contribution to $F_m$ exceeds the contribution of UFP to $F_m$ by a large amount. Mass deposition fluxes of approximately −0.05 µg $m^{-2}$ $s^{-1}$ occur mostly in the afternoon at around 15:00, whereas fluxes during the night and early morning hours fluctuate around zero. Thus, deposition mostly occurs between 11:00–20:00 (Fig. 3b). The deposition shows notable synchronicity to turbulence as approximated by the momentum flux, with simultaneous peaks around 15:00. The increasing turbulence intensity as well as the increasing boundary layer height with the possible entrainment from the overlying residual layer are thus likely drivers of turbulent transport of particles into the city. The normalized flux distribution (Fig. 6) shows the variation of the flux direction and its magnitude as a function of particle diameters. For the mass fluxes, particles of $D_m$ = 106 nm (channel 8) contribute most to emissions, whereas particles of $D_m$ = 301 nm (channel 18) lead to maximum deposition. The tipping point between emission and deposition is, again, at 167 nm. Negative fluxes are on average three times larger than emission fluxes, leading to an average weekday deposition of −53 µg $m^{-2}$ $d^{-1}$. The average Sunday deposition (−0.08 µg $m^{-2}$ $d^{-1}$) is considerably smaller than on weekdays, which also indicates that fluxes of particles in the 167–300 nm size range are highly influenced by workday activity.

## 3.3 Urban-Rural comparison

To test our flux data for wind direction effects, we compared fluxes from three source sectors, representing the following land use categories: (1) rural, (2) industry and traffic, and (3) traffic and residential. According to the above described tipping point, we further divided the data into two groups, one for the smaller (< 167 nm) and the other for the bigger particles.

No significant differences between the magnitudes of fluxes from sectors 2 and 3 were identified (with sector 2, $\bar{F}_{n<167} \approx 9.3 \cdot 10^6$ $m^{-2}$ $s^{-1}$and sector 3, $\bar{F}_{n<167} \approx 9.1 \cdot 10^6$ $m^{-2}$ $s^{-1}$, respectively). However, sector 1 small-particle fluxes were significantly ($p < 0.01$) smaller than fluxes of sector 2 and 3 (Wilcoxon-Mann-Whitney-Test), with a mean of $\bar{F}_{n<167} \approx 3.7 \cdot 10^6$ $m^{-2}$ $s^{-1}$.

This is only true for the smaller particles, while bigger particles were not sensitive to the wind direction classification. This result suggests that even though the two urban classification sectors feature substantially different emission sources (sector 2 hosts potentially large emitters such as an inland harbor, industrial funnels and a power plant), the bulk of particles responsible for the number fluxes are produced throughout the entire city. We conclude that traffic emissions are the main fine particle emitters in Münster and that industrial emissions only play a minor role for the magnitude of $F_n$. The significantly lower $F_{n<167}$ of the rural/suburban sector 1 further supports the often reported observation that air masses from more rurally stamped source regions exhibit significantly lower particle loadings and fluxes (MÅRTENSSON et al., 2006; JÄRVI et al., 2009; VOGT et al., 2011a). Furthermore, the results suggest that particles $D_m > 167$ nm are rather of a supra-regional character, insensitive to an urban/rural classification. This is in good agreement with the autocorrelation analysis presented above, with results from impactor samples (GIETL et al., 2008; HARRISON et al. 2011) and with mass spectroscopy studies (ALLAN et al., 2003; NEMITZ et al., 2008), confirming that accumulation mode particles contain mainly secondary compounds associated with regional and long range transport patterns.

## 4 Summary and conclusion

The application of an optical particle spectrometer in combination with the EC method allows size-resolved particle flux measurements with a size resolution of 19 channels ranging from 55–1000 nm. The study revealed that the city of Münster acts as a distinct source for particles with a mean daily emission of $2.49 \cdot 10^8$ $m^{-2}$ $d^{-1}$ for the given particle size range. However, this is just a result of the simultaneous occurrence of fluxes from two distinct particle regimes having an opposite sign (upward or downward). Emission is mostly driven by UFP, while bigger particles in the accumulation mode (167–1000 nm) are the main source of deposition. The highly size-resolved approach of this study allowed the quantification of the tipping point (167 nm) between these regimes within a precision of 20 nm. The observation of bi-directional fluxes as a function of particle size is in good agreement with results of an earlier study of SCHMIDT and KLEMM (2008). However, those authors found a considerably larger tipping point of 320 nm. The cause for this disagreement may lie in their different experimental phase potentially representing different particle populations, and in the different measurement approaches and instruments employed here. Nevertheless, it can be noted that both studies found tipping points within the accumulation mode.

Furthermore, our results conform with particle source apportionment studies at urban street level sites. It is found that a portion of the particles in the urban environment originates from distant sources while another portion is produced within the city environment itself (GIETL and KLEMM, 2009). These portions do not only differ in particle size, but also in their chemical composition (ALLAN et al., 2003; NEMITZ et al., 2008; HARRISON et al. 2011). Our concept of bi-directional fluxes in the urban canopy layer perfectly matches this image. Particles with diameters $D_m < 167$ nm show a distinct diurnal behavior, and they are the main contributors to the positive number fluxes, $F_n$. The respective ambient concentrations change rather rapidly, at time scales of a few hours. The $F_n$ of urban footprints are significantly higher than those from rural ones. We conclude that the positive $F_n$ are mainly driven by urban traffic emissions. In contrast, the mostly downward transported particles with diameters $D_m > 167$ nm appear to be subject to larger temporal and spatial scales. The respective number fluxes $F_n$ ($D_m > 167$ nm) were not sensitive to a footprint classification. A timescale analysis revealed that the concentrations of these particles have a high persistency. We conclude that it is mainly meso-scale advection and down-mixing of aged particulate material that lead to the observed deposition fluxes of the larger particles. Note that the downward flux of the larger particles leads to a net deposition of particle mass to the urban environment in our experiment.

More studies, covering longer experimental periods, in both different climates and urban structures are required to shed more light on these processes.

To minimize the uncertainties and further enhance the quality of particle fluxes, future instrumentation development should not only aim to increase the size resolution of OPCs, but more importantly to focus on increasing the maximum count limitations for one single measurement interval.

## Acknowledgments

This study was supported by the German Science Foundation (DFG) through contract KL623/12. We further thank Roland BALTHASAR on behalf of the Bundeswehr for the possibility to use their radio tower. Furthermore, we would like to thank T. EL-MADANY, S. SANTOS and ILÖK staff for support during field work. Language-editing by L. HARRIS is much appreciated. Last but not least we thank two anonymous reviewers for very helpful comments on an earlier version of the manuscript.

## References

AHLM, L., R. KREJCI, E.D. NILSSON, E.M. MÅRTENSSON, M. VOGT, P. ARTAXO, 2010: Emission and dry deposition of accumulation mode particles in the Amazon Basin. – ACPD **10**, 10237–10253.

ALLAN, J.D., M.R. ALFARRA, K.N. BOWER, P.I. WILLIAMS, M.W. GALLAGHER, J.L. JIMENEZ, A.G. MCDONALD, E. NEMITZ, M.R. CANAGARATNA, J.T. JAYNE, H. COE,

D.R. WORSNOP, 2003: Quantitative sampling using an Aerodyne aerosol mass spectrometer. 2. Measurements of fine particulate chemical composition in two U.K. cities. – J. Geophys. Res. **108**, 4091.

ASMI, A., A. WIEDENSOHLER, P. LAJ, A.-M. FJAERAA, K. SELLEGRI, W. BIRMILI, E. WEINGARTNER, U. BALTENSPERGER, V. ZDIMAL, N. ZIKOVA, J.-P. PUTAUD, A. MARINONI, P. TUNVED, H.-C. HANSSON, M. FIEBIG, N. KIVEKÄS, H. LIHAVAINEN, E. ASMI, V. ULEVICIUS, P.P. AALTO, E. SWIETLICKI, A. KRISTENSSON, N. MIHALOPOULOS, N. KALIVITIS, I. KALAPOV, G. KISS, G. DE LEEUW, B. HENZING, R.M. HARRISON, D. BEDDOWS, C. O'DOWD, S.G. JENNINGS, H. FLENTJE, K. WEINHOLD, F. MEINHARDT, L. RIES, M. KULMALA, 2011: Number size distributions and seasonality of submircron particles in Europe 2008–2009. – Atmos. Chem. Phys. **11**, 5505–5538.

BARON, P.A., K. WILLEKE, 2005: Aerosol Measurement: Principles, Techniques, and Applications. – John Wiley & Sons, New York. 1160 pp..

BUZORIUS, G., Ü. RANNIK, E.D. NILSSON, T. VESALA, M. KULMALA, 2003: Analysis of measurement techniques to determine dry deposition velocities of aerosol particles with diameters less than 100 nm. – J. Aerosol Sci. **34**, 747–764.

DAHLKÖTTER, F., F. GRIESSBAUM, A. SCHMIDT, O. KLEMM, 2010: Direct measurement of $CO_2$ and particle emissions from an urban area. – Meteorol. Z. **19**, 565–575.

DORSEY, J.R., E. NEMITZ, M.W. GALLAGHER, D. FOWLER, P.I. WILLIAMS, K.N. BOWER, K.M. BESWICK, 2002: Direct measurements and parameterisation of aerosol flux, concentration and emission velocity above a city. – Atmos. Environ. **36**, 791–800.

FAIRALL, C.W., 1984: Interpretation of eddy-correlation measurements of particulate deposition and aerosol flux. – Atmos. Environ. **18**, 1329–1337.

FOKEN, T., B. WICHURA, 1996: Tools for quality assessment of surface-based flux measurements. – Agrar. Forest Meteor. **78**, 83–105.

GIETL, J.K., O. KLEMM, 2009: Source identification of size-segregated aerosol in Münster, Germany, by factor analysis. – Aerosol Sci. Tech. **43**, 828–837.

GIETL, J.K., T. TRITSCHER, O. KLEMM, 2008: Size-segregated analysis of PM10 at two sites, urban and rural, in Münster (Germany) using five-stage Berner type impactors. – Atmos. Environ. **42**, 5721–5727.

GRIESSBAUM, F., A. SCHMIDT, 2009: Advanced tilt correction from flow distortion effects on turbulent $CO_2$ fluxes in complex environments using large eddy simulation. – Quart. J. Roy. Meteor. Soc. **135**, 1603–1613.

HARRISON, R.M., M. DALL'OSTO, D.C.S. BEDDOWS, A.J. THORPE, W.J. BLOSS, J.D. ALLAN, H. COE, J.R. DORSEY, M. GALLAGHER, C. MARTIN, J. WHITEHEAD, P.I. WILLIAMS, R.L. JONES, J.M. LANGRIDGE, A.K. BENTON, S.M. BALL, B. LANGFORD, C.N. HEWITT, B. DAVISON, D. MARTIN, K. PETERSSON, S.J. HENSHAW, I.R. WHITE, D.E. SHALLCROSS, J.F. BARLOW, T. DUNBAR, F. DAVIES, E. NEMITZ, G.J. PHILLIPS, C. HELFTER, C.F. DI MARCO, S. SMITH, 2011: Atmospheric chemistry and physics in the atmosphere of a developed megacity (London): an overview of the REPARTEE experiment and its conclusions. – Atmos. Chem. Phys. **12**, 3065–3114.

HINDS, W.C., 1999: Aerosol Technology. Properties, Behavior, and Measurement of Airborne Particles, John Wiley & Sons, New York, 504 pp.

IPCC, 2007: Climate Change 2007: The physical science basis. Contribution of Working Group I to the Fourth Assessment Report of the Intergovernmental Panel on Climate Change. – Cambridge University Press, Cambridge, 996 pp.

JÄRVI, L., Ü. RANNIK, I. MAMMARELLA, A. SOGACHEV, P.P. AALTO, P. KERONEN, E. SIIVOLA, M. KULMALA, T. VESALA, 2009: Annual particle flux observations over a heterogeneous urban area. – Atmos. Chem. Phys. **9**, 7847–7856.

KULMALA, M., H. VEHKAMÄKI, T. PETÄJÄ, M. DAL MASO, A. LAURI, V.M. KERMINEN, W. BIRMILI, P.H. MCMURRY, 2004: Formation and growth rates of ultrafine atmospheric particles: a review of observations. – J. Aerosol Sci. **35**, 143–176.

LENSCHOW, D.H., L. KRISTENSEN, 1984: Uncorrelated Noise in Turbulence Measurements. – J. Atmos. Oceanic Tech. **2**, 68–81.

MÅRTENSSON, E.M., E.D. NILSSON, G. BUZORIUS, C. JOHANSSON, 2006: Eddy covariance measurements and parameterization of traffic related particle emissions in an urban environment. – Atmos. Chem. Phys. **6**, 769–785.

MARTIN, C.L., I.D. LONGLEY, J.R. DORSEY, R.M. THOMAS, M.W. GALLAGHER, E. NEMITZ, 2009: Ultrafine particle fluxes above four major European cities. – Atmos. Environ. **43**, 4714–4721.

MAUDERLY, J.L., J.C. CHOW, 2008: Health effects of organic aerosols. – Inhal. Toxicol. **20**, 257–288.

NEMITZ, E., D. FOWLER, J.R. DORSEY, M.R. THEOBALD, A.D. MCDONALD, K.N. BOWER, K.M. BESWICK, P.I. WILLIAMS, M.W. GALLAGHER, 2000: Direct measurements of size-segregated Particle fluxes above a city. – J. Aerosol. Sci. **31**, 116–118.

NEMITZ, E., J.L. JIMENEZ, J.A. HUFFMAN, I.M. ULBRICH, M.R. CANAGARATNA, D.R. WORSNOP, A.B. GUENTHER, 2008: An Eddy-Covariance System for the Measurement of Surface/Atmosphere Exchange Fluxes of Submicron Aerosol Chemical Species – First Application Above an Urban Area. – Aerosol Sci. Tech. **42**, 636–657.

PITZ, M., J. CYRYS, E. KARG, A. WIEDENSOHLER, H.E. WICHMANN, J. HEINRICH, 2003: Variability of Apparent Particle Density of an Urban Aerosol. – Environ. Sci. & Tech. **37**, 4336–4342.

QUEROL, X., A. ALASTUEY, S. RODRIGUEZ, F. PLANA, C.R. RUIZ, N. COTS, G. MASSAGUE, O. PUIG, 2001: PM10 and PM2.5 source apportionment in the Barcelona Metropolitan area, Catalonia, Spain. – Atmos. Environ. **35**, 6407–6419.

SALMA, I., T. BORSÓS, T. WEIDINGER, P. AALTO, T. HUSSEIN, M. DAL MASO, M. KULMALA, 2011: Production, growth and properties of ultrafine atmospheric aerosol particles in an urban environment. – Atmos. Chem. Phys. **11**, 1339–1353.

SCHMID, H.P., 1994: Source areas for scalars and scalar fluxes. – Bound.-Layer Meteor. **67**, 293–318.

SCHMIDT, A., O. KLEMM, 2008: Direct determination of highly size-resolved turbulent particle fluxes with the disjunct eddy covariance method and a 12-stage electrical low pressure impactor. – Atmos. Chem. Phys. **8**, 7405–7417.

SWIETLICKI, E., S. PURI, H.C. HANSSON, H. EDNER, 1996: Urban air pollution source apportionment using a combination of aerosol and gas monitoring techniques. – Atmos. Environ. **30**, 2795–2809.

TAYLOR, J.R., 1982: An introduction to error analysis. – University science books, Mill Valley(CA), 327 pp.

VICKERS, D., L. MAHRT, 1997: Quality control and flux sampling problems for tower and aircraft data. – J. Atmos. Ocean. Technol. **14**, 512–526.

VOGT, M., E.D. NILSSON, L. AHLM, E.M. MÅRTENSSON, C. JOHANSSON, 2011a: The relationship between 0.25-2.5 mu m aerosol and CO(2) emissions over a city. – Atmos. Chem. Phys. **11**, 4851–4859.

VOGT, M., E.D. NILSSON, L. AHLM, E.M. MÅRTENSSON, C. JOHANSSON, 2011b: Seasonal and diurnal cycleso of 0.25–2.5 um aerosol fluxes over urban Stockholm, Sweden. – Tellus **63**(B), 935–951.

WEBB, E.K., G.I. PEARMAN, R. LEUNING, 1980: Correction of flux measurements for density effects due to heat and water vapor transfer. – Quart. J. Roy. Meteor. Soc. **106**, 85–100.